Journal of Power Sources 212 (2012) 247–253

Contents lists available at SciVerse ScienceDirect

Journal of Power Sources

journal homepage: www.elsevier.com/locate/jpowsour

Improved ceramic anodes for SOFCs with modified electrode/electrolyte interface

A. Mohammed Hussain*, Jens V.T. Høgh, Wei Zhang, Eugen Stamate, Karl T.S. Thydén, Nikolaos Bonanos

DTU Energy Conversion (formerly known as 'Risø National Laboratory for Sustainable Energy'), Department of Energy Conversion and Storage, Risø Campus, Technical University of Denmark, Roskilde 4000, Denmark

ARTICLE INFO

Article history:
Received 17 January 2012
Received in revised form
27 March 2012
Accepted 30 March 2012
Available online 13 April 2012

Keywords:
Metal functional layer
Palladium nanoparticles
Electrode/electrolyte interface
Pd–CGO electrocatalysts
Infiltrations
Low temperature SOFC anodes

ABSTRACT

The electrode performance of solid oxide fuel cell anode with Pd nanoparticles at the interface of ScYSZ electrolyte and $Sr_{0.94}Ti_{0.9}Nb_{0.1}O_3$ (STN) electrode introduced in the form of metal functional layer have been investigated at temperatures below 600 °C. A metal functional layer consisting of Pd was deposited by magnetron sputtering. Effecting from heat treatments, Pd nanoparticles with particle sizes in the range of 5–20 nm were distributed at the interface, and throughout the backbone. The polarization resistance of the modified STN reduced to 30 Ωcm^2 at 600 °C, which is three times less than an unmodified STN backbone. In order to improve the anode performance further, Pd and Gd-doped CeO_2 electrocatalysts were infiltrated into the STN backbone. The modified interface with Pd nanoparticles in combination with nanostructured electrocatalyst by infiltration resulted in polarisation resistances of 0.35 Ωcm^2 at 600 °C in H_2/3% H_2O fuel.

1. Introduction

Conventional anodes for solid oxide fuel cells (SOFCs) consist of a cermet of nickel and yttrium-stabilized zirconia (YSZ) [1–3]. Although Ni–YSZ cermet has excellent electrochemical properties for hydrogen oxidation, it has the drawback of high polarization resistance at low temperatures (<600 °C) and poor redox stability [4,5]. High performing alternative anodes are required to overcome the limitations of Ni–YSZ cermets for low temperature SOFC (LT-SOFC) applications [6].

Recently, ceramic based materials have been extensively studied for LT-SOFCs, e.g. $Sr_{0.94}Ti_{0.9}Nb_{0.1}O_3$ (STN) perovskite type oxides. In spite of their low oxide ion conductivity and poor catalytic activity for hydrogen oxidation, these oxides have excellent electronic conductivity and redox stability [7]. Various attempts have been made to use doped-$SrTiO_3$ as a potential LT-SOFC anode. A composite of YSZ or $La_{0.8}Sr_{0.2}Ga_{0.8}Mg_{0.2}O_{2.8}$ (LSGM) with Y-doped $SrTiO_3$ has been tried [8]. While composites of STN/YSZ would probably provide the necessary oxide ion transport; these cannot be used for SOFC anodes without further modification, due to their high polarization resistances (R_p) [7].

When pure electronic material like STN is used as anode, the electrochemical reactions are confined to the electrode/electrolyte interfaces (EEI) [9], where electrode, electrolyte and the fuel gas are in contact forming a three phase boundary (TPB). Incorporation of nanostructured, catalytically active sites and path for oxide ion conduction is necessary in extending the TPBs [10]. TPB length plays a crucial role in improving the performance of SOFC anodes. Moreover, introducing electrocatalyst such as Ni and Gd-doped ceria (CGO) by infiltration is proven to extend the TPB length and to improve the performances [11–14].

The main goal of this study is to improve the performance of STN based anodes by introducing catalyst nanoparticles at the EEI i.e., nanosized Pd catalyst was incorporated in the required site of hydrogen oxidation in the form of a metal functional layer (MFL). The study was made systematic by varying the thickness of MFL deposited at the interface with the aim to increase the loading of catalyst; however the best performance is achieved with a MFL of 20 and 30 nm. The combined beneficial effects of Pd–CGO electrocatalyst infiltration and distributed Pd nanoparticles at the interface have shown a drastic improvement in electrode performance at low temperatures.

* Corresponding author. Tel.: +45 46775639; fax: +45 46775858.
E-mail addresses: abhu@risoe.dtu.dk, uzzain@gmail.com (A.M. Hussain).

0378-7753/$ – see front matter © 2012 Elsevier B.V. All rights reserved.
doi:10.1016/j.jpowsour.2012.03.110

2. Experimental

2.1. Deposition of metal functional layer (MFL) using magnetron sputtering

An MFL was deposited by magnetron sputtering technique on both sides of pre-sintered ScYSZ (10 mol% Sc_2O_3 in 1 mol% Y_2O_3 stabilized ZrO_2) electrolyte tape to form a symmetrical cell. The magnetron sputtering setup consisted of a vacuum chamber evacuated up to 10^{-6} Torr with a set of roughing and turbo molecular pumps. Ar gas was fed using a mass flow controller to create a working pressure (p), of tens of m Torr. The magnetron sputtering cathode (2 inch in diameter) with indirect water cooling and possibility of both RF excitation and DC bias was produced by Kurt Lesker. In present experiments a palladium plate of 0.2 mm in thickness and 50 mm in diameter was bound with a thermally conductive silver adhesive on a thicker copper disc. The resulted target was DC biased (U_{DC}) with more than 200 V to ignite the plasma discharge, while measuring the discharge current (I_D). Ions produced by electron ionization in the plasma-ring following the magnetic field of the cathode were accelerated towards the target (biased negatively) striking its surface with energies of over 100 eV. The ion impacts produce physical sputtering of atoms and clusters from the target and are then transported by diffusion on the substrate forming a film. A ScYSZ electrolyte tape with an area of 6×6 cm^2 and 120 μm thick was used as a substrate to deposit MFL. Typical parameters were $p = 50$ m Torr, $U_{DC} = 360$ V, $I_D = 200$ mA with a deposition rate of 20 nm min^{-1}. Deposition times of 60, 90, 300 and 500 s were used to deposit films of thickness 20, 30, 100 and 170 nm, respectively. The thickness of the films was determined using a Veeco stylus profilometer. The initial structure of the symmetrical cells was MFL | ScYSZ electrolyte | MFL.

2.2. Fabrication of symmetrical cells

The STN powders synthesized by wet chemical method reported elsewhere [15,16]. Backbones of STN was prepared by screen printing an in-house STN ink on both the sides of ScYSZ electrolyte deposited with MFL to form a STN | MFL | ScYSZ electrolyte | MFL | STN structure. This raw symmetrical cell was sintered in air (1100–1300 °C) for 4 h. Subsequently, the sintered symmetrical cell was pre-reduced at 1000 °C in H_2/N_2 gas for 5 h. These heat treatments resulted in distribution of MFL into nanoparticles at EEI. The tape was cut into smaller pieces having an electrode area of 0.25 cm^2 for use in the electrochemical set-up. The porosity of the STN backbone was determined from the SEM images of the polished samples using simple phase analysis software.

A 0.75 M CGO ($Ce_{0.8}Gd_{0.2}O_{2-\delta}$) precursor solution were prepared by dissolving cerium nitrate ($Ce(NO_3)_3{\cdot}6H_2O$) and gadolinium nitrate ($Gd(NO_3)_3{\cdot}6H_2O$) in water along with a polymer surfactants to improve wetting properties. A precursor solution of Pd–CGO was made by mixing 0.60 M palladium nitrate ($Pd(NO_3)_2{\cdot}6H_2O$) in an already prepared CGO solution. Pd–CGO precursor solution contains 10 wt.% of Pd and 90 wt.% of CGO. The STN anodes were prepared by infiltrating few drops of the prepared precursor solution into the symmetrical cell, after which they were placed in a vacuum chamber. Vacuum was applied in order to remove the air bubbles and facilitate the liquid precursor penetrate the anode homogeneously. The cell was infiltrated 3 times with Pd–CGO; after each infiltration the cells were calcined at 350 °C for 1 h in air. The change in weight after calcination was recorded after each infiltration. The formation of fluorite type structure of CGO was confirmed using XRD analysis and no reaction occurred between CGO and PdO. The volume fraction of Pd–CGO is 7.6 vol.% in STN | MFL | ScYSZ electrolyte | MFL | STN, while 8.5 vol.% for STN | ScYSZ electrolyte | STN symmetrical cell.

2.3. Electrochemical characterizations

A Solartron SI1260 frequency response analyser was used to measure the impedance of the symmetrical cells. The symmetrical cells were electrically contacted using Pt-paste (Ferro GmbH) and a Pt-grid. The polarization resistance of Pt-paste as anode is very high (123 Ωcm^2 at 650 °C in H_2/3% H_2O) owing to their larger grain sizes and lack of oxide ion conductivity. The contribution from Pt current collector is negligible and the same current collector was used for all the anodes to compare the results [17]. The cells were heated to 650 °C in dry gas mixtures of 9% H_2/N_2, where after the gas was changed to dry H_2 and the temperature were kept at 650 °C for 12 h. The impedance spectra were recorded at open circuit conditions (OCV) by applying amplitude of 50 mV (the output voltage of the Solartron varies from 5–50 mV depending on the temperature i.e., the cell impedance) in the frequency range of 1–5 MHz. The impedance was measured in the temperature range from 650 to 350 °C in H_2/3% H_2O. The gas compositions were made by humidifying H_2 in a water bubbler at room temperature. The partial pressure of oxygen, (pO_2) was measured using an oxygen sensor. The EMF values were −1.131, −1.138, −1.145 and −1.147 V vs. air, corresponding to pO_2 values of 10^{-26}, 10^{-27}, 10^{-29}, and 10^{-31} atm at 650, 600, 550 and 500 °C, respectively. These value corresponds very well with the gas composition of 97% H_2/3% H_2O. The impedance data were corrected for inductances originating from the leads of electrochemical setup (30–60 nH depending on the electrode), determined on the cells in short circuit at room temperature. The impedance spectra were fitted with an equivalent circuit using ZSimpWin with a complex non-linear least squares fitting routine (CNLS).

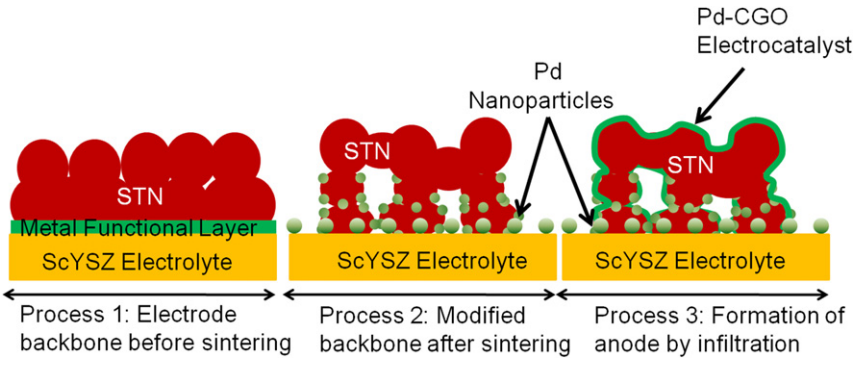

Fig. 1. Schematic sketch illustrating the structure of SOFC anode.

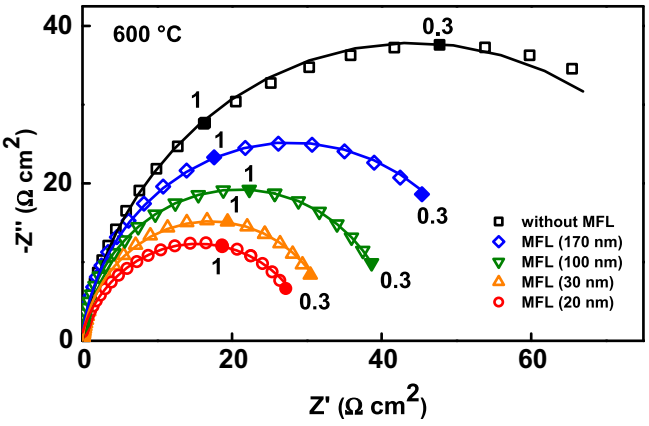

Fig. 2. Impedance spectra for hydrogen oxidation measured at 600 °C with metal functional layer (MFL) of different thicknesses and without MFL. The numbers in the spectra indicate the frequencies, in Hz. The electrolyte series resistance are subtracted from the spectra and the solid lines connecting the measured data points indicate the equivalent circuit fits.

2.4. Microstructure and elemental analysis

The microstructure of the EEI was investigated with a transmission electron microscope (TEM) at an accelerating voltage of 300 kV (JEM-3000F, FEGTEM). An energy dispersive X-ray spectra (EDX) analysis was performed on the particles located in the EEI using an Oxford EDS detector. A thin TEM lamella was prepared by use of a FIB–TEM H-bar technique in a crossbeam 1540XB dual focused ion beam (FIB)/SEM from Carl Ziess.

3. Results and discussion

Fig. 1 is the schematic sketch of the anode structure used in this work. Process 1, before sintering portray the raw assembly (one side of the symmetrical cell is shown), wherein MFL is sandwiched between the printed STN and pre-sintered ScYSZ tape. Process 2 corresponds to distribution of Pd thin film into nanoparticles at the EEI and on the STN backbone after sintering and process 3 illustrates the infiltrated Pd–CGO electrocatalyst into the STN backbone forming a percolated network of Pd–CGO.

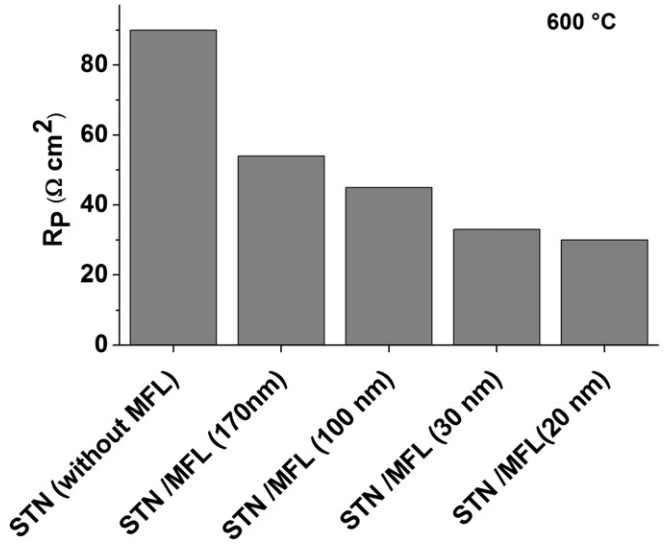

Fig. 3. Bar chart illustrating the reduction in anode polarization resistance for a STN anode with metal functional layer (MFL) measured at 600 °C in 3%H_2/H_2O.

Shown in Fig. 2 are the impedance spectra of STN symmetrical cells with and without MFL measured at 600 °C. The high frequency intercept in the X-axis corresponds to the ohmic resistance of the electrolyte (R_s). In the spectra shown, the values of R_s and polarization resistance (R_p) were determined from the impedance spectra fitted using the general equivalent circuits R_s (R_pQ_p). The bar chart shown in Fig. 3 illustrates the R_p values obtained from the impedance spectra. The impedance of STN without Pd shows a high R_p of 90 Ωcm^2. With a Pd MFL of 170 nm at the EEI, R_p reduces to 54 Ωcm^2. A thinner MFL at the interface yielded better performance. This can be seen from the impedance spectra for various MFL thicknesses ranging from 20 to 170 nm. For instance, with 100 and 30 nm thick MFL, R_p reduces to 45 and 33 Ωcm^2, respectively i.e., for thin films below 100 nm, 40–50% reductions in R_p was achieved at 600 °C. The performance of 30 nm MFL is similar to that of 20 nm MFL, which is about 30 Ωcm^2. With a 20 nm thick MFL, R_p reduction of 70% is achieved to that of unmodified STN. Although a considerable reduction in R_p is achieved by incorporating MFL, a further reduction in STN anodes are required and can be achieved

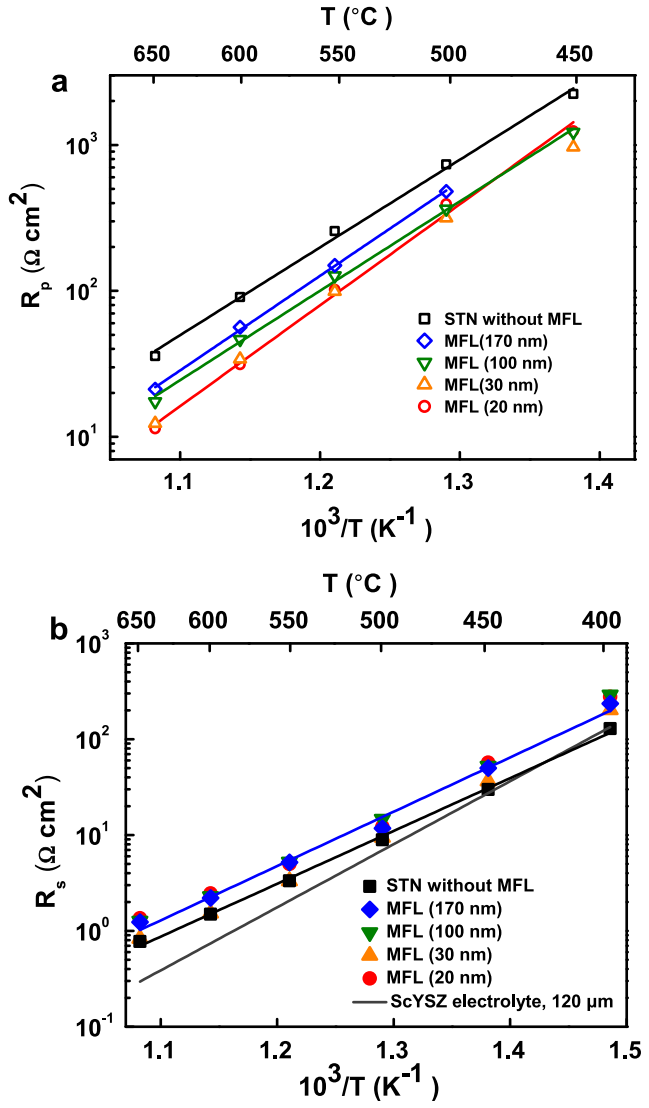

Fig. 4. a) Arrhenius plot of polarization resistance (R_p) and b) temperature dependency plot of electrolyte ohmic resistance (R_s). The straight line represents the ohmic resistance of ScYSZ electrolyte with a thickness of 120 μm calculated from the conductivity values reported in literature.

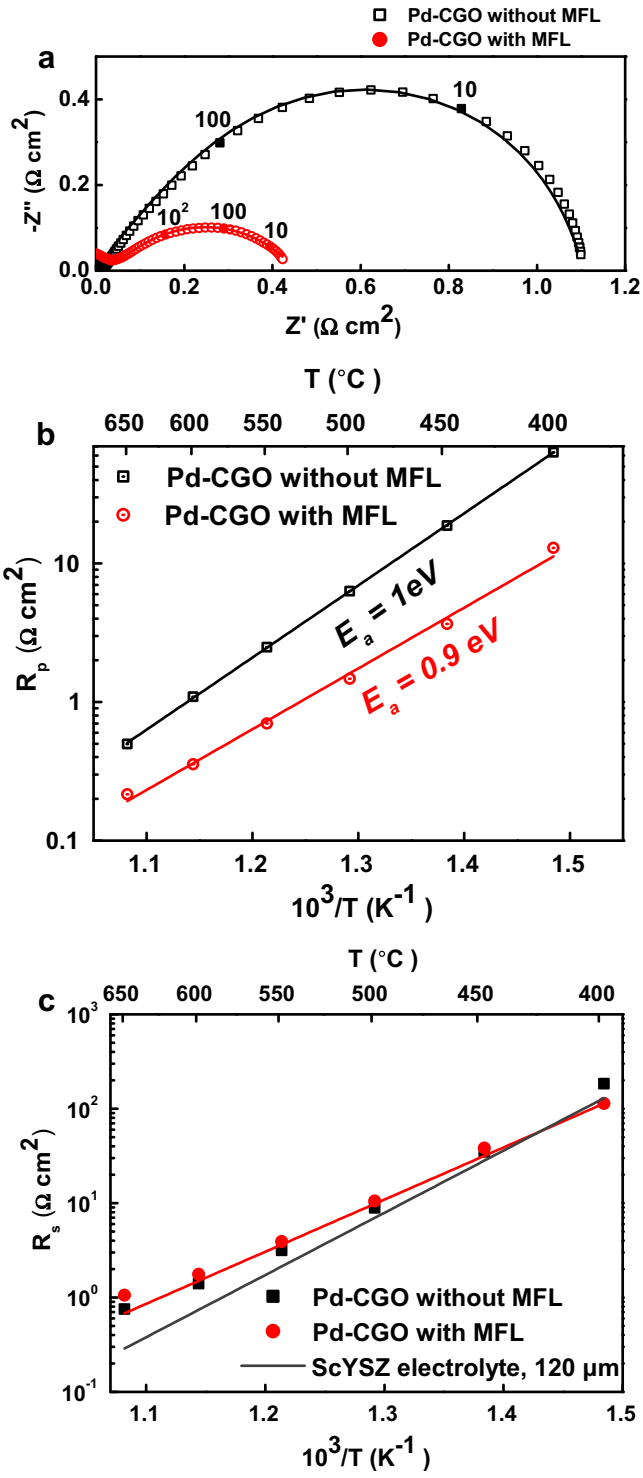

Fig. 5. a) Impedance spectra of Pd–CGO infiltrated STN anodes with and without metal functional layer (MFL) measured at 600 °C in moisturized hydrogen. The numbers in the spectra indicate the frequencies, in Hz. The electrolyte series resistance is subtracted from the spectra and the solid lines connecting the measured data points indicate the equivalent circuit fits. b) Arrhenius plot of polarization resistance (R_p) and c) Temperature dependency plot of electrolyte ohmic resistance (R_s). The straight line represents the ohmic resistance of ScYSZ electrolyte with a thickness of 120 μm calculated from the conductivity values reported in literature.

only with the introduction of electrocatalyst by infiltration into the STN backbone.

Shown in Fig. 4a is the Arrhenius plot of R_p. The activation energy (E_a) was determined and is in the range of 0.95–1.00 eV for all anodes, both with or without MFL and irrespective of its thickness, despite the variation in polarization resistance. Fig. 4b shows the temperature dependence of R_s. A comparison of R_s with an ohmic resistance of ScYSZ electrolyte is shown. The ionic conductivity values of ScYSZ electrolyte were adopted from the literature [18] and calculated based on the electrolyte thickness of 120 μm. The random variations of the electrolyte ohmic resistance between the different electrodes are thought to originate from any improper contact of the current collector and from the microstructural variations of the electrode in contact with electrolyte.

Table. 1
Electrode polarization resistance and summit frequencies obtained from the equivalent circuit analysis of the impedance spectra at 600 °C in H_2/H_2O.

STN Backbone	R_0 (Ωcm^2)	$F_{max,\ 0}$ (Hz)	R_1 (Ωcm^2)	$F_{max,\ 1}$ (Hz)	R_2 (Ωcm^2)	$F_{max,\ 2}$ (Hz)	R_p (Ωcm^2)
Pd–CGO electrocatalyst w/o MFL	–	–	0.3	105	0.8	4.3	1.1
Pd–CGO electrocatalyst with MFL(20 nm)	0.1	2×10^5	0.35	507	–	–	0.35

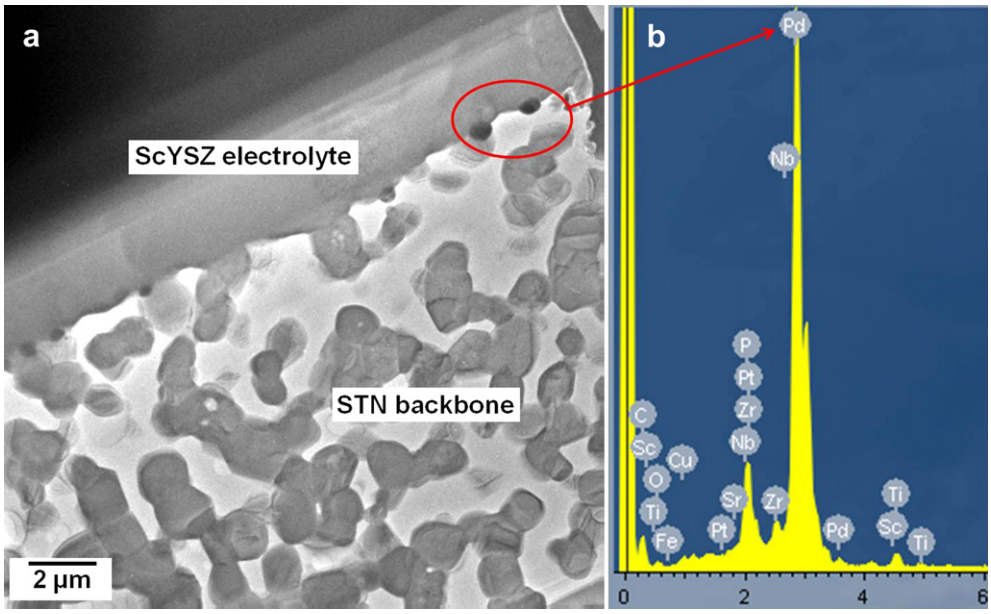

Fig. 6. TEM image of the STN symmetrical cells with metal functional layer (MFL). a) Illustration of the Pd nanoparticles at the interface of STN backbone and ScYSZ electrolyte and b) Energy dispersive X-ray spectroscopy (EDX) analysis on the nanoparticles.

Fig. 5a shows the impedance spectra of Pd–CGO infiltrated STN backbone with and without MFL of 20 nm thickness measured at 600 °C. Equivalent circuits $R_0^{'}$ (R_0Q_0) (R_1Q_1) and R_s (R_1Q_1) (R_2Q_2) were used to determine $R_s(=R_0^{'}+R_0)$ and $R_p\ (=R_1+R_2)$. The fitted parameters such as resistance (R), admittance parameter (Y_0), and frequency power (n) for each (RQ) sub-circuits were used to calculate the characteristic frequency (F_{max}) using the relations 1.

$$F_{max} = \frac{1}{(R\cdot Q)^{1/n}\cdot 2\cdot\pi} \quad (1)$$

The equivalent circuit fitted parameters of the anode at 600 °C are listed in Table 1. The R_p of Pd–CGO electrocatalyst infiltrated STN is 1.1 Ωcm^2 and for an infiltrated backbone with Pd nanoparticles at the EEI, R_p has been reduced to 0.35 Ωcm^2, which is a 65% reduction. The performance of these electrodes was compared with almost similar loading (8 vol.%) of Pd–CGO electrocatalyst.

Pd–CGO electrocatalyst infiltrated STN without MFL was fitted with an equivalent circuit containing the sub-circuits (R_1Q_1) and (R_2Q_2) i.e., R_s (R_1Q_1) (R_2Q_2). The former sub-circuit in high frequency part (100–500 Hz) of the spectrum represents the charge transfer resistance at the electrode/electrolyte interface, while the latter sub-circuit at low frequency part (5–10 Hz) represents the impedance due to dissociative adsorption in combination with gas diffusion limitations [19–21]. However, the gas phase diffusion impedance must be very small compared to the impedance of other electrode processes. In case of Pd–CGO infiltrated with Pd MFL of 20 nm thickness, (R_0Q_0) and (R_1Q_1) i.e. $R_0^{'}$ (R_0Q_0) (R_1Q_1) equivalent circuit was used to fit the spectrum. (R_0Q_0) at very high frequency part (10 kHz) of spectrum is not an electrode related process and represents the bulk properties of electrolyte. This can be supported from low capacitance (0.8 μF cm) and by observing the impedance spectra at low temperatures, where impedance arcs ascribed to grain boundary and grain interior fall within the frequency range of the impedance analyser. As suggested earlier, the sub-circuit (R_2Q_2) is linked to electrode process in combination [19,21]. A drastic improvement in charge transfer in combination with dissociative adsorption of hydrogen is observed in these modified electrodes. The presence of gas diffusion impedances at low frequencies (10 Hz) slightly appears at this temperature and is more evident at high temperature measurements.

The Arrhenius plot of R_p is shown in Fig. 5b. The E_a of the Pd–CGO infiltrates STN anode without MFL is 1 eV and for the anode with MFL a similar E_a of 0.9 eV is obtained. Shown in Fig. 5c are the temperature dependencies of R_s. The calculated E_a are 1.26 and 1.3 eV for STN anodes and ScYSZ electrolyte, respectively [18].

The role of the MFL in improving the performance of the STN based anodes was investigated using TEM. Hydrogen oxidation in STN was expected to take place only at the interface and modification at interface with high surface area catalyst is proven beneficial [9]. Figs. 6 and 7 gives an overview of STN electrode with 30 nm Pd MFL in the EEI. Fig. 6a is the cross section of STN/ScYSZ symmetrical cell. Close examination at the interface of ScYSZ electrolyte and STN backbone reveals dark spots of Pd nanoparticles and they are about 20 nm in size. Furthermore, STN backbone adheres well with the ScYSZ electrolyte. Fig. 6b shows the presence of Pd peak at 2.84 keV resulted from an EDX point analysis on these dark sites.

Further elemental analysis on STN/ScYSZ interface shown in Fig. 7a reveals the nanoparticles of Pd at the interface and on the STN backbone (shown in Fig. 7b). The size of the Pd particles is small i.e., less than 5 nm. During sintering in air, the Pd thin film oxidizes and is expected to form PdO agglomerates. It is believed that a fraction of the PdO migrates along with the STN powder particles, while other fraction remains on the ScYSZ electrolyte. Following sintering, a treatment in H_2/N_2 gas conditions at 1000 °C would convert the PdO into Pd particles. Shown in Fig. 8a and b (high resolution image) is the Pd–CGO infiltrated STN anode in combination with Pd nanoparticles. The

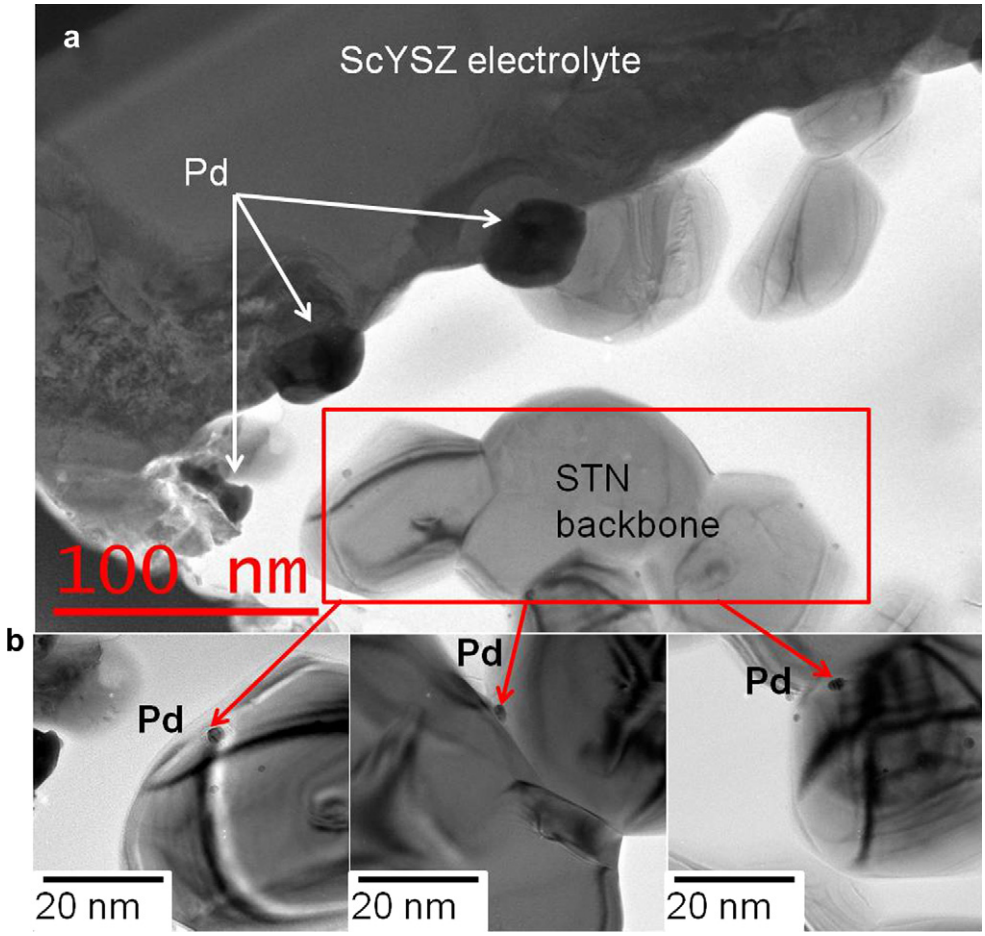

Fig. 7. TEM images of the STN backbone showing the distribution of MFL after sintering. a) STN/ScYSZ interface with distributed Pd nanoparticles and b) Three images shows the presence of nanosized Pd on the STN backbone.

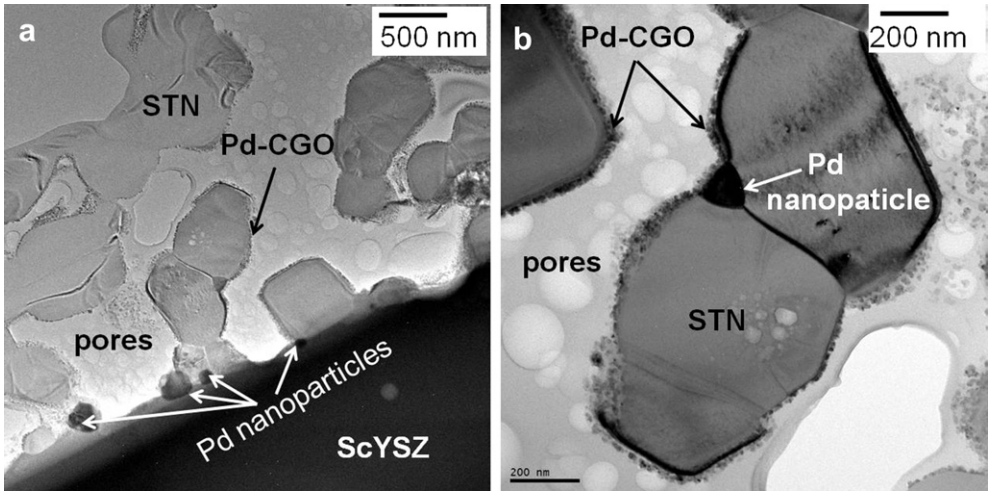

Fig. 8. TEM images a) STN anode showing nanostructured Pd–CGO electrocatalyst in combination with Pd nanoparticles. b) High magnification image (part of Fig. 8a).

image shown in Fig. 8a clearly reveals the distribution of Pd nanoparticles at the interface and demonstrates that they uniformly cover STN backbone. It is suggested from Fig. 8b that Pd–CGO has the particles size distribution smaller than the Pd nanoparticles, which may have resulted in a better electrode performance.

4. Conclusions

The electrochemical properties of $Sr_{0.94}Ti_{0.9}Nb_{0.1}O_3$ ceramic backbone as SOFC anodes were improved by a Pd nanoparticles at the interface of electrode and electrolyte. The catalytic activity is still

insufficient to attain a decent SOFC anode performance at low temperatures of SOFC. Hence, the anode is further infiltrated with Pd–CGO electrocatalyst, which resulted in a drastic reduction of electrode polarization resistance. The combination of interface modification with Pd–CGO electrocatalyst infiltrations had shown an improved electrode performance of 0.35 Ωcm^2. The microstructural analysis on the electrode revealed the presence of nanosized electrocatalyst with two different particle size distributions.

Acknowledgements

The authors wish to thank Ebtisam Abdellahi for TEM sample preparations. Financial support from the Department of Energy Conversion and Storage within the project SOFC400 is gratefully acknowledged

References

[1] M. Mogensen, K.V. Jensen, M.J. Jørgensen, S. Primdahl, Solid State Ionics 150 (2002) 123–129.
[2] T. Iwata, J. Electrochem. Soc. 143 (1996) 1521.
[3] H. Koide, Y. Someya, T. Yoshida, T. Maruyama, Solid State Ionics 132 (2000) 253–260.
[4] T. Fukui, K. Murata, S. Ohara, H. Abe, M. Naito, K. Nogi, J. Power Sources 125 (2004) 17–21.
[5] O. Costa-Nunes, R.J. Gorte, J.M. Vohs, J. Power Sources 141 (2005) 241–249.
[6] H. Kurokawa, L. Yang, C.P. Jacobson, L.C. De Jonghe, S.J. Visco, J. Power Sources 164 (2007) 510–518.
[7] P. Blennow, A. Hagen, K.K. Hansen, L. Wallenberg, M. Mogensen, Solid State Ionics 179 (2008) 2047–2058.
[8] S. Hui, A. Petric, J. Eur. Ceram. Soc. 22 (2002) 1673–1681.
[9] M. Brown, S. Primdahl, M. Mogensen, J. Electrochem. Soc. 147 (2000) 475.
[10] M.A. Laguna-Bercero, Á Larrea, R.I. Merino, J.I. Peña, V.M. Orera, J. Am. Ceram. Soc. 88 (2005) 3215–3217.
[11] P. Blennow, K.K. Hansen, L.R. Wallenberg, M. Mogensen, ECS Trans. 13 (2008) 181–194.
[12] W. Zhu, D. Ding, C. Xia, Electrochem. Solid-State Lett. 11 (2008) B83.
[13] D. Ding, W. Zhu, J. Gao, C. Xia, J. Power Sources 179 (2008) 177–185.
[14] A. Mohammed Hussain, J.V.T. Høgh, T. Jacobsen, N. Bonanos, Int. J. Hydrogen Energy 37 (2012) 4309.
[15] M. Jain, S. Majumder, R. Guo, A. Bhalla, R. Katiyar, Mater. Lett. 56 (2002) 692–697.
[16] F.A. Rabuffetti, H.S. Kim, J.A. Enterkin, Y. Wang, C.H. Lanier, L.D. Marks, et al., Chem. Mater. 20 (2008) 5628–5635.
[17] U.P. Muecke, K. Akiba, A. Infortuna, T. Salkus, N.V. Stus, L.J. Gauckler, Solid State Ionics 178 (2008) 1762–1768.
[18] M. Laguna-Bercero, S. Skinner, J. Kilner, J. Power Sources 192 (2009) 126–131.
[19] A. Babaei, S.P. Jiang, J. Li, J. Electrochem. Soc. 156 (2009) B1022–B1029.
[20] A. Leonide, KIT Scientific Publishing, 2009, ISBN 978-3-86644-538-3, 54–56.
[21] Y. Nabae, I. Yamanaka, M. Hatano, K. Otsuka, SOFC modelling and parameter identification by means of impedance spectroscopy. J. Electrochem. Soc. 153 (2006) A140.